Geophysical Research Letters

Supporting Information for

Gas hydrate dissociation during sea-level highstand inferred from U/Th dating of seep carbonate from the South China Sea

Fang Chen [1,†], Xudong Wang [2,3,4,9,†], Niu Li [3], Jun Cao [1], Germain Bayon [4], Jörn Peckmann [5], Yu Hu [6], Shanggui Gong [6], Hai Cheng [7,8], R. Lawrence Edwards [7], Youfeng Ning [8], Meng Jin [3,9], Huiwen Huang [3,9], Cong Wu [1], Yuedong Sun [3,9], Hong Chen [1], Yang Zhou [1], Duofu Chen [2,6], Dong Feng [2,6*]

[1]MNR Key Laboratory of Marine Mineral Resources, Guangzhou Marine Geological Survey, Ministry of Natural Resources, Guangzhou, Guangdong 510075, China, [2]Laboratory for Marine Mineral Resources, Qingdao National Laboratory for Marine Science and Technology, Qingdao 266061, China, [3]CAS Key Laboratory of Ocean and Marginal Sea Geology, South China Sea Institute of Oceanology, Chinese Academy of Sciences, Guangzhou 510301, China, [4]IFREMER, Marine Geosciences Unit F-29280 Plouzané, France, [5]Institute for Geology, Center for Earth System Research and Sustainability, Universität Hamburg, Hamburg 20146, Germany, [6]Shanghai Engineering Research Center of Hadal Science and Technology, College of Marine Sciences, Shanghai Ocean University, Shanghai 201306, China, [7]Department of Earth Sciences, University of Minnesota, Minneapolis, MN, 55455, USA, [8]Institute of Global Environmental Change, Xi'an Jiaotong University, Xi'an 710054, China, [9]University of Chinese Academy of Sciences, Beijing 100049, China

Contents of this file

Revision submitted to *Geophysical Research Letters*

Text S1. Method for XRD and stable carbon and oxygen isotopes analysis

The X-ray source was a Cu anode operated at 40 kV and 300 mA using CuKα radiation equipped with a diffracted beam graphite monochromator. The samples were scanned by a step scan mode at an interval of 2-65° (2θ), with a step size of 0.01° and a count time of 1 s per step. The diverging, scattering, and receiving slits were 1.0 mm, 1.0 mm and 0.15 mm, respectively. Rietveld refinement was performed by using XRD processing software JADE 6.0 programs to analyze the content of various mineral components in carbonate.

Carbon and oxygen stable isotopes of hand-drilled carbonates were analyzed with a GasBench II preparation line connected to a Thermo Finnigan MAT253 mass spectrometer (Thermo Scientific, USA). The powdered carbonate samples were first treated with 100% phosphoric acid at 80 °C to release CO_2 for analysis. The reproducibility better than ±0.1‰ for $\delta^{13}C$ and $\delta^{18}O$ values. Stable isotopic compositions are reported in conventional delta (δ) notation relative to the Vienna-Pee Dee Belemnite (VPDB) standard.

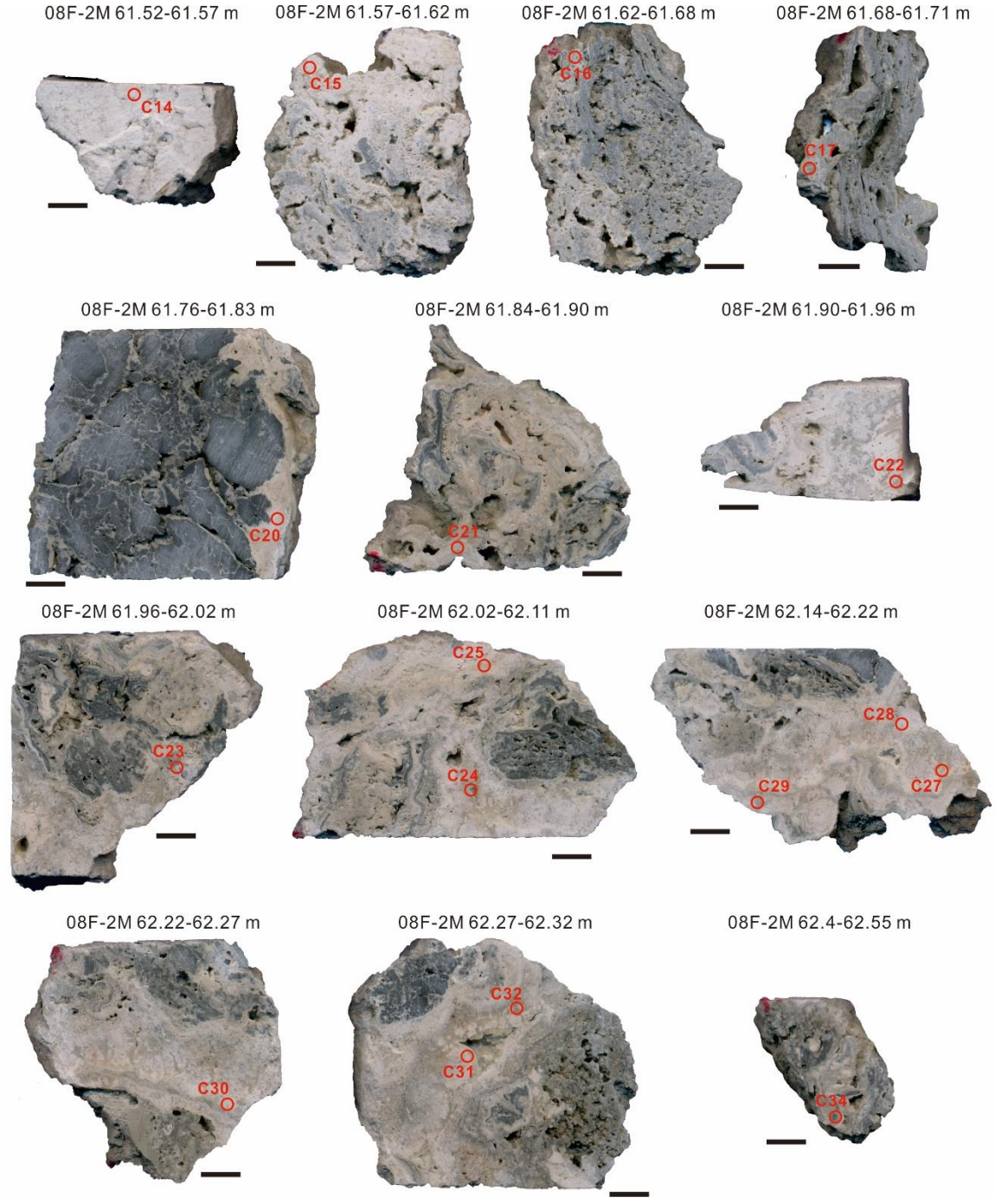

Figure S1. Seep carbonates from core 8F with U/Th sample locations. The depth (meter below the seafloor) of samples are indicated on top of the images. The scale bars are 1 cm.

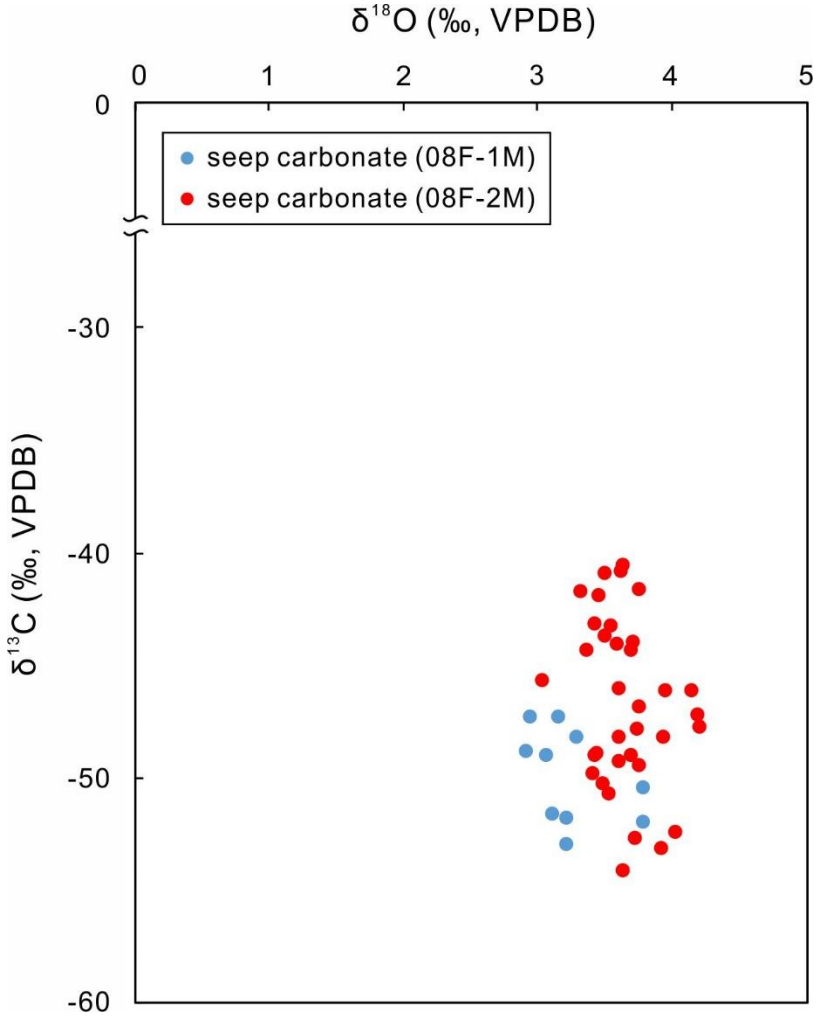

Figure S2. Carbon and oxygen stable isotopes of seep carbonate.

Table S1. Mineralogical compositions of seep carbonates.

Core	Number	Depth (mbsf)	Mineral composition (%)									
			LMC	HMC	Mn-calcite	Aragonite	Dolomite	Fe-dolomte	Quartz	Feldspar	Clay	Magnesite
08F-1M	1	58.95-59.00		1.6		86.7			4.4	2.6	4.8	
	2	59.00-59.04		0.6		93.5						3.4
	3	59.04-59.10		1.5		82.3			3.1	0.1	13	
	4	59.07-59.13		3.4		80.9			6.1	1.9	7.3	
	5	59.11-59.18		1.2		89.8			1.6		7.3	
	6	59.16-59.21		1.5		85.4			3.4	1.6	8.1	
	7	59.21-59.25		0.9		87			2.5		8.8	0.9
	8	59.24-59.32	0.6			96.6					2.8	
	9	59.26-59.31		2		87.2			0.1		8	2.7
	10	59.34-59.46		1.5		86.4			3.3	0.2	8.6	
08F-2M	11	61.52-61.57	6.4			91.8						1.8
	12	61.52-61.57	5			87.7			3		3.7	0.5
	13	61.57-61.62	3.5			96.3	0.2					
	14	61.57-61.62	5.3			91.7	0.2		2.8			
	15	61.76-61.83		10.9	6	32.2		19.7	9	4.1	15.9	2.2
	16	61.76-61.83	5.4			94.5	0.1					0.2
	17	61.96-62.02	4.8			95	0.1					0.1
	18	61.96-62.02	8.4			73.7		1.7	5.1	1.6	8.7	0.8
	19	62.02-62.11	7.7			80.9			3.7		7	0.8
	20	62.02-62.11	4.6			95						0.4
	21	62.02-62.11	3.9			95.6					0.2	0.3
	22	62.14-62.22	5.8			94	0.1					0.1
	23	62.14-62.22		21.3	13.8	33.2			9	3.2	19.5	
	24	62.40-62.55	4.6			91.3			3.7		0.3	0.1
	25	62.40-62.55		22	0.2	41.2		10.6	9.5	6.4	9.9	0.1

LMC, low-magnesium calcite. HMC, high-magnesium calcite.

Table S2. Carbon and oxygen stable isotopes of seep carbonate layers (o8F-1M + o8F-2M) from gas hydrate drilling core of the South China Sea.

Core	Number	Depth (mbsf)	$\delta^{13}C$ (‰, VPDB)	$\delta^{18}O$ (‰, VPDB)
08F-1M	1	58.95-59.00	-49.0	3.1
	2	59.00-59.04	-51.5	3.1
	3	59.04-59.10	-47.2	2.9
	4	59.07-59.13	-47.2	3.1
	5	59.11-59.18	-48.8	2.9
	6	59.16-59.21	-52.9	3.2
	7	59.21-59.25	-51.7	3.2
	8	59.24-59.32	-50.4	3.8
	9	59.26-59.31	-51.9	3.8
	10	59.34-59.46	-48.1	3.3
08F-2M	11	61.52-61.57	-41.6	3.3
	12	61.52-61.57	-52.6	3.7
	13	61.57-61.62	-46.8	3.7
	14	61.57-61.62	-48.9	3.4
	15	61.62-61.68	-49.2	3.6
	16	61.62-61.68	-46.1	3.9
	17	61.68-61.71	-48.9	3.7
	18	61.68-61.71	-49.8	3.4
	19	61.71-61.76	-47.1	4.2
	20	61.71-61.76	-49.4	3.7
	21	61.76-61.83	-46.0	4.1
	22	61.76-61.83	-47.7	3.7
	23	61.84-61.90	-43.1	3.4
	24	61.84-61.90	-43.9	3.7
	25	61.84-61.90	-46.0	3.6
	26	61.90-61.96	-41.6	3.7
	27	61.90-61.96	-48.8	3.4
	28	61.96-62.02	-40.5	3.6
	29	61.96-62.02	-52.3	4.0
	30	62.02-62.11	-53.0	3.9
	31	62.02-62.11	-40.8	3.5
	32	62.02-62.11	-40.7	3.6
	33	62.11-62.14	-45.6	3.0
	34	62.11-62.14	-50.7	3.5
	35	62.14-62.22	-43.6	3.5
	36	62.14-62.22	-48.1	3.9
	37	62.22-62.27	-54.1	3.6
	38	62.22-62.27	-41.8	3.4
	39	62.27-62.32	-48.1	3.6
	40	62.27-62.32	-43.2	3.5
	41	62.27-62.32	-44.2	3.7

42	62.32-62.40	-44.0	3.6
43	62.32-62.40	-44.3	3.4
44	62.40-62.55	-50.2	3.5
45	62.40-62.55	-47.7	4.2

Table S3. U-Th isotopic data and calculated ages of seep carbonates.

Core	Sample ID[a]	Depth (mbsf)	^{238}U (ppb)	^{232}Th (ppt)	^{230}Th / ^{232}Th (atomic × 10^{-6})	$\delta^{234}U$[b] (measured)	^{230}Th / ^{238}U (activity)	^{230}Th Age (ka BP) (uncorrected)	^{230}Th Age (ka BP)[c] (corrected)	$\delta^{234}U_{Initial}$[d] (corrected)
08F-1M	C1	58.95-59.00	5618 ± 7	673 ± 18	103182 ± 2821	106.6 ± 1.3	0.7500 ± 0.0013	120.2 ± 0.5	120.1 ± 0.5	150 ± 2
	C2	59.00-59.04	8837 ± 14	2871 ± 59	37176 ± 769	104.6 ± 1.5	0.7326 ± 0.0014	115.7 ± 0.5	115.6 ± 0.5	145 ± 2
	C3	59.05-59.15	6399 ± 18	42927 ± 866	1851 ± 37	109.5 ± 1.7	0.7531 ± 0.0024	120.4 ± 0.8	120.2 ± 0.8	154 ± 2
	C4	59.15-59.20	9174 ± 10	8492 ± 170	12850 ± 258	103.8 ± 1.2	0.7214 ± 0.0011	112.8 ± 0.4	112.7 ± 0.4	143 ± 2
	C5	59.20-59.25	670 4± 7	6874 ± 138	11706 ± 236	98.1 ± 1.3	0.7281 ± 0.0011	115.8 ± 0.4	115.7 ± 0.4	136 ± 2
	C6	59.26-59.31	8011 ± 9	7171 ± 144	13922 ± 280	99.0 ± 1.4	0.7559 ± 0.0011	123.6 ± 0.5	123.5 ± 0.5	140 ± 2
	C7	59.28-59.35	6045 ± 6	16517 ± 331	4482 ± 90	100.4 ± 1.4	0.7427 ± 0.0009	119.5 ± 0.4	119.3 ± 0.4	141 ± 2
	C8	59.28-59.35	5941 ± 7	1707 ± 36	44248 ± 928	98.0 ± 1.4	0.7713 ± 0.0011	128.5 ± 0.5	128.4 ± 0.5	141 ± 2
	C9	59.35-59.45	9060 ± 11	5281 ± 107	21154 ± 429	93.9 ± 1.4	0.7479 ± 0.0012	122.4 ± 0.5	122.3 ± 0.5	133 ± 2
	C10	59.35-59.45	6076 ± 8	4871 ± 98	15667 ± 315	98.2 ± 1.3	0.7618 ± 0.0013	125.6 ± 0.5	125.5 ± 0.5	140 ± 2
	M1	59.35-59.45	8275 ± 31	506562 ± 10298	210 ± 4	99.6 ± 3.1	0.7791 ± 0.0032	130.6 ± 1.3	128.9 ± 1.7	143 ± 5
	C11	59.48	4808 ± 4	31263 ± 626	1952 ± 39	103.4 ± 1.2	0.7699 ± 0.0010	126.8 ± 0.4	126.5 ± 0.4	148 ± 2
	M2	59.48	6421 ± 19	317408 ± 6410	261 ± 5	98.4 ± 2.4	0.7823 ± 0.0027	131.9 ± 1.1	130.6 ± 1.4	142 ± 4
08E	C12	61.00-61.10	3276 ± 3	201 ± 13	209132 ± 13200	98.7 ± 1.3	0.7792 ± 0.0012	130.8 ± 0.5	130.8 ± 0.5	143 ± 2
08F-2M	C13	61.15-61.30	6070 ± 12	3030 ± 61	25471 ± 518	102.2 ± 1.4	0.7712 ± 0.0019	127.5 ± 0.7	127.4 ± 0.7	146 ± 2
	C14	61.52-61.57	5914 ± 7	2839 ± 57	24888 ± 503	96.7 ± 1.4	0.7247 ± 0.0011	115.2 ± 0.4	115.1 ± 0.4	134 ± 2
	C15	61.57-61.62	5959 ± 7	2130 ± 44	34676 ± 717	95.9 ± 1.3	0.7519 ± 0.0015	123.1 ± 0.5	123.1 ± 0.5	136 ± 2
	C16	61.62-61.68	6024 ± 7	13177 ± 264	5817 ± 117	98.0 ± 1.3	0.7718 ± 0.0012	128.7 ± 0.5	128.6 ± 0.5	141 ± 2
	C17	61.68-61.71	6202 ± 8	19987 ± 401	3850 ± 77	96.5 ± 1.3	0.7524 ± 0.0013	123.2 ± 0.5	123.0 ± 0.5	137 ± 2
	C18	61.68-61.71	5537 ± 10	7504 ± 151	8937 ± 180	96.2 ± 1.7	0.7346 ± 0.0015	118.1 ± 0.6	118.0 ± 0.6	134 ± 2
	C19	61.71-61.76	5939 ± 7	44927 ± 900	1629 ± 33	97.3 ± 1.4	0.7475 ± 0.0012	121.5 ± 0.5	121.3 ± 0.5	137 ± 2
	M3	61.71-61.76	4548 ± 13	2880168 ± 58238	22 ± 0.44	96.0 ± 3.0	0.8313 ± 0.0032	149.6 ± 1.5	132.0 ± 12.6	139 ± 7
	C20	61.76-61.83	6037 ± 8	2185 ± 45	35535 ± 740	96.3 ± 1.4	0.7801 ± 0.0014	131.7 ± 0.6	131.7 ± 0.6	140 ± 2
	C21	61.84-61.90	5485 ± 6	4227 ± 85	16778 ± 338	95.3 ± 1.3	0.7843 ± 0.0012	133.4 ± 0.5	133.3 ± 0.5	139 ± 2
	C22	61.90-61.96	6583 ± 9	756 ± 17	110576 ± 2443	99.0 ± 1.5	0.7701 ± 0.0014	127.9 ± 0.6	127.8 ± 0.6	142 ± 2
	C23	61.96-62.02	5037 ± 6	2662 ± 55	24337 ± 501	97.6 ± 1.3	0.7801 ± 0.0012	131.4 ± 0.5	131.3 ± 0.5	141 ± 2

C24	62.02-62.11	5569 ± 8	867 ± 18	82489 ± 1746	98.0 ± 1.5	0.7786 ± 0.0013	130.8 ± 0.5	130.8 ± 0.5	142 ± 2
C25	62.02-62.11	5508 ± 7	1425 ± 30	49955 ± 1047	95.6 ± 1.4	0.7841 ± 0.0013	133.2 ± 0.6	133.2 ± 0.6	139 ± 2
C26	62.11-62.14	5986 ± 7	567 ± 13	135693 ± 3144	97.5 ± 1.3	0.7794 ± 0.0012	131.2 ± 0.5	131.1 ± 0.5	141 ± 2
C27	62.14-62.22	7835 ± 11	2101 ± 44	47800 ± 1000	98.7 ± 1.4	0.7772 ± 0.0014	130.2 ± 0.6	130.1 ± 0.6	143 ± 2
C28	62.14-62.22	4606 ± 6	1580 ± 33	37379 ± 777	96.9 ± 1.4	0.7777 ± 0.0013	130.8 ± 0.5	130.7 ± 0.5	140 ± 2
C29	62.14-62.22	7242 ± 10	11721 ± 235	7920 ± 159	99.0 ± 1.4	0.7775 ± 0.0012	130.2 ± 0.5	130.1 ± 0.5	143 ± 2
C30	62.22-62.27	5737 ± 6	2920 ± 59	24043 ± 486	96.0 ± 1.2	0.7421 ± 0.0014	120.3 ± 0.5	120.2 ± 0.5	135 ± 2
C31	62.27-62.32	4881 ± 8	2127 ± 43	27632 ± 565	99.1 ± 1.7	0.7303 ± 0.0015	116.2 ± 0.5	116.2 ± 0.5	138 ± 2
C32	62.27-62.32	5082 ± 6	3382 ± 68	19015 ± 386	96.5 ± 1.4	0.7676 ± 0.0013	127.8 ± 0.5	127.7 ± 0.5	138 ± 2
C33	62.27-62.32	5037 ± 5	3745 ± 75	17242 ± 347	98.5 ± 1.3	0.7775 ± 0.0010	130.3 ± 0.5	130.3 ± 0.5	142 ± 2
M4	62.32-62.40	7111 ± 23	2919940 ± 59139	33 ± 1	104.3 ± 2.9	0.8234 ± 0.0031	144.0 ± 1.4	133.1 ± 7.8	152 ± 5
C34	62.40-62.55	4593 ± 6	8109 ± 163	7251 ± 146	95.5 ± 1.5	0.7765 ± 0.0013	130.8 ± 0.6	130.7 ± 0.6	138 ± 2
C35	62.40-62.55	4745 ± 6	2795 ± 57	21836 ± 442	97.2 ± 1.4	0.7800 ± 0.0013	131.5 ± 0.5	131.4 ± 0.5	141 ± 2
M5	62.40-62.55	2306 ± 4	1667918 ± 33451	19 ± 0.38	102.3 ± 1.7	0.8336 ± 0.0024	148.3 ± 1.1	128.3 ± 14.4	147 ± 6
C36	62.55-62.70	7678 ± 9	8291 ± 167	11338 ± 228	98.0 ± 1.4	0.7425 ± 0.0012	119.9 ± 0.5	119.8 ± 0.5	138 ± 2

U decay constants: $\lambda_{238} = 1.55125 \times 10^{-10}$ (Jaffey et al., 1971) and $\lambda_{234} = 2.82206 \times 10^{-6}$ (Cheng et al., 2013). Th decay constant: $\lambda_{230} = 9.1705 \times 10^{-6}$ (Cheng et al., 2013). Corrected ^{230}Th ages assume the initial $^{230}Th/^{232}Th$ atomic ratio of $4.4 \pm 2.2 \times 10^{-6}$. Those are the values for a material at secular equilibrium, with the bulk earth $^{232}Th/^{238}U$ value of 3.8. The errors are arbitrarily assumed to be 50%. The uncertainties of our age data are quoted at 2σ.

a: C = cement; M = microcrystalline matrix.

b: $\delta^{234}U = ([^{234}U/^{238}U]_{activity} - 1) \times 1000$.

c: B.P. stands for "Before Present" where the "Present" is defined as the year 1950 A.D.

d: $\delta^{234}U_{initial}$ was calculated based on ^{230}Th age (T), i.e., $\delta^{234}U_{initial} = \delta^{234}U_{measured} \times e^{\lambda_{234} \times T}$.

Table S4. Compilation of published U-Th dating results of global seep carbonates.

No.	Location	water depth (m)	Sample ID	Best Age (ka)	Reference
1	the eastern part of Nankai accretionary prism	2190	KN19-1 mould	27.5±2	Lalou et al., 1992
		1950	KN 6-5 mould	22.5±2.2	
		2062	KN 15-7 cement	> 350	
		2062	KN 15-7 mould	> 350	
		2190	KN 14-1 mould	44.6±1.7	
		3689	K1 External part	116±16	
			K2 center	98±12	
			K3 intermediate	20±1.7	
2	the Gulf of Mexico	152	89-5-2/a	52.5 ± 2.8	Aharon et al., 1997
		260	89-9-5/a	99.3 ± 6.5	
			89-9-5/b	93.9 ± 12.9	
			89-11-1/a(M)	38.9 ± 3.1	
			89-11-1/a(C)	38.9 ± 3.1	
		267	88-26-3/a	194.9 ± 23.1	
		598	89-12-1/b(M)	3.2 ± 1.9	
			89-12-1/b(C)	1.4 ± 1.4	
		2200	90-2209-R(C)	8.5 ± 2.9	
3	Hydrate Ridge, Cascadia Margin	788	21-2-B-1	1.3 ± 0.4	Teichert et al., 2003
		788	21-2-B-2	1.3 ± 0.2	
		787	55-5-3	0.8 ± 0.9	
		787	56-1-C-2	3.4 ± 0.3	
		787	56-1-C-1	1.8 ± 0.7	
		787	56-1-C-5	4.3 ± 0.4	
		787	56-1-H-1	4.8 ± 0.7	
		787	56-1-H-2	6.4 ± 0.8	
		772	222-C-1	1.4 ± 0.3	
		766	571-3-3	0.8 ± 0.3	
		774	3428-6-A-1	10.9 ± 0.6	
		812	3424-4-A-2	7.3 ± 0.2	
		772	3429-3-A-2	9.2 ± 0.3	
		772	3429-3-A-8a	8.8 ± 2.0	
		772	3429-3-A-8b	11.4 ± 1.0	
		762	570-1-3	8.5 ± 0.1	
		776	571-2-1	9.7 ± 0.3	
		776	571-2-2	9.8 ± 1.2	
		762	570-9-5	10.9 ± 0.2	
		620	26	267.6 ± 5.5	

		620	26-1	177.7 ± 4.2	
		620	26-3	221.7 ± 4.5	
		616	565-7-7	22.3 ± 0.7	
		668	36-4-Z-1	68.7 ± 1.4	
		668	36-4-Z-2	71.7 ± 0.6	
		924	60-1-Eb, calcite	1.4 ± 0.3	
4	the middle slope offshore Central America	1000 - 1500	M66-184	8.3 ± 0.2	Kutterolf et al., 2008
			M66-129	65.6 ± 1.6	
			M66-129	32.1 ± 0.5	
			M66-157	70.3 ± 1.3	
			M66-157	55.8 ± 1.6	
5	off Joetsu, Eastern Margin of Japan Sea	900	PC05-02-60	21.7 ± 7.1	Watanabe et al., 2008
			PC05-04-50(1)	25.3 ± 2.9	
			PC05-04-50(2)	25.2 ± 2.2	
			PC05-04-50(3)	24.6 ± 3.2	
			PC05-04-65	62.4 ± 2.6	
			PC05-CC(1)	21.3 ± 1.4	
			PC05-CC(2)	21.5 ± 1.5	
			PC05-CC(3)	21.6 ± 1.5	
			PC15-04-00	35.8 ± 4.5	
			PC15-04-30	21.4 ± 5.4	
			PC15-06-1(b)	22 ± 2.0	
			PC15-06-1(c)	23.1 ± 1.7	
			PC15-06-2(1)	12.8 ± 2.7	
			PC15-06-2(2)	13.6 ± 3.2	
			PC15-06-2(3)	15.8 ± 2.7	
			PC15-06-3(1)	20.6 ± 4.9	
			PC15-06-3(2)	21.5 ± 4.4	
			G3	35.3 ± 3.5	
6	the Central Nile deep sea fan	2130	NL14-CC5 (2cm)	7.9 ± 1.4	Bayon et al., 2009b
7	offshore Egypt, on the Nile deep-sea fan (Eastern Mediterranean basin)	~ 1650	0.0cm	9.1 ± 2.5	Bayon et al., 2009a
			0.1cm	4.9 ± 1.2	
			0.4cm	3.5 ± 2.1	
			0.9cm	2.8 ± 1.3	
			1.0cm	2.5 ± 1.4	
			2.2cm	2.95 ± 0.88	
			2.5cm	2.2 ± 1.0	
			2.5cm	2.0 ± 1.4	
			replicate	1.8 ± 1.5	
			2.8cm	2.6 ± 1.4	
			3.6cm	2.06 ± 0.93	

			4.3cm	2.1 ± 1.3	
			5.0cm	0.8 ± 1.3	
			5.5cm	0.8 ± 1.3	
8	the Bay of Bengal, offshore India	1033	carbonate tubules at 16 mbsf	46.2 ± 3.7 to 53 ± 1.6 ka	Mazumdar et al., 2009
9	the Gulf of Mexico	2230	4194-1	53.4 ± 0.9	Feng et al., 2010
			4194-2	2.55 ± 5	
			4194-3	45 ± 1	
			4194-4	16 ± 2	
			4197-1	14.2 ± 0.9	
			4197-2	11.3 ± 0.1	
			4197-3	9.3 ± 0.6	
			4197-4	8.6 ± 0.3	
			4197-5	10.4 ± 0.5	
			4197-6	11.1 ± 0.5	
			281-1	11.7 ± 0.5	
		2240	4180-1	10 ± 1	
			4180-2	7.9 ± 0.1	
			4180-3	8.0 ± 0.1	
			4180-4	12 ± 2	
			4180-5	8.0 ± 0.1	
			4183-1	9.9 ± 0.1	
			270-1	6.2 ± 0.2	
			270-3	5.8 ± 0.2	
			270-6	3.1 ± 0.2	
			270-8	2.9 ± 0.1	
			277-1	1.6 ± 0.1	
	Congo Fan	3100	HH-2a-1-1	3.0 ± 0.9	
			HH-2a-1-2	6 ± 2	
			HH-2a-2-1	29 ± 9	
			HH-2a-2-2	30 ± 10	
			HH-2a-3-1	50 ± 10	
			HH-2a-3-2	40 ± 10	
			HH-2d-1-1	15 ± 5	
			HH-2d-1-2	18 ± 6	
			HH-2d-1-3	17 ± 6	
			HH-2d-1-4	21 ± 7	
		2400	DF-2c-1	22 ± 5	
			DF-2c-2	23 ± 6	
			DF-2c-3	23 ± 6	
	Black Sea	120	RO-1	1.6 ± 0.6	

			RO-2	1.5 ± 0.2	
			RO-3	1.1 ± 0.1	
		180 - 200	UKR-1	0.5 ± 0.9	
			UKR-2	0.9 ± 0.1	
			UKR-3	1.2 ± 0.1	
10	the Hikurangi Margin, New Zealand	1047	138-1	2.92 ± 0.19	Liebetrau et al., 2010
			138-2	2.67 ± 0.03	
			138-3	2.53 ± 0.02	
			138-4	2.39 ± 0.04	
			138-5	3.96 ± 0.05	
			138-6	4.26 ± 0.04	
			138-7	3.36 ± 0.48	
			138-8	4.27 ± 0.05	
			138-9	4.29 ± 0.04	
			138-10	4.95 ± 0.65	
			138-11	0.23 ± 0.02	
		756	316-1	4.12 ± 0.04	
			316-2	4.31 ± 0.04	
			316-3	12.40 ± 0.16	
		1102	165-1	2.36 ± 0.07	
			165-2	2.09 ± 0.85	
11	the Mediterranean Sea	1118	BN-122-CC2	8.9 ± 2.8	Bayon et al., 2013
			BN-122-CC3-1	1.3 ± 0.4	
			BN-122-CC3-2	1.3 ± 0.9	
			BN-122-CC4-1	10.0 ± 0.2	
			BN-122-CC4-3	10.0 ± 0.9	
			BN-122-CC4-5	11.2 ± 1.4	
			BN-122-CC4-2	8.9 ± 0.2	
			BN-122-CC4-4	7.4 ± 0.1	
			BN-122-CC5-1	7.5 ± 0.4	
			BN-122-CC5-2	8.0 ± 0.7	
			BN-122-CC6-1	7.3 ± 0.2	
			BN-122-CC6-2	7.8 ± 0.2	
			BN-122-CC8	9.8 ± 2.5	
			BN-123-CC1-1	8.8 ± 3.7	
			BN-123-CC1-2	7.3 ± 1.0	
			BN-123-CC2-1	7.7 ± 2.0	
			BN-123-CC2-2	11.7 ± 5.1	
			BN-123-CC3-1	11.2 ± 6.8	
			BN-123-CC3-2	10.7 ± 3.9	
			BN-123-CC4	8.4 ± 3.1	

12	the Sea of Marmara	> 1000	1647-R1 a	1.01 ± 0.3	Crémière et al., 2013
			1647-R1 b	1.83 ± 0.15	
			1667-R1 a	0.63 ± 0.03	
			1667-R1 b	3.47 ± 0.56	
			1661-R2	3.92 ± 0.87	
			1653-R3	6.63 ± 0.52	
			1653-R5	0.43 ± 0.06	
			1662-R1 a	5.19 ± 0.75	
			1662-R1 b	6.50 ± 0.87	
			1662-R4	1.30 ± 0.31	
			1662-R5	2.19 ± 0.09	
			1669-BB	1.48 ± 0.61	
			1664-R1	3.28 ± 0.19	
		~ 660	MNT-KS14, 0.98 msbf a	10.17 ± 0.33	
			MNT-KS14, 0.98 msbf b	8.63 ± 0.16	
			MNT-KS14, 0.98 msbf c	9.95 ± 0.52	
			MNT-KS14, 1.03 mbsf	6.30 ± 0.23	
			MNT-KS14, 1.08 mbsf a	9.50 ± 0.27	
			MNT-KS14, 1.08 mbsf b	9.76 ± 0.5	
			MNT-KS14, 1.08 mbsf c	11.40 ± 1.1	
			MNT-KS14, 1.08 mbsf d	8.90 ± 0.43	
			MNT-KS14, 1.08 mbsf e	8.92 ± 0.16	
			MNT-KS14, 1.08 mbsf f	8.06 ± 0.46	
			MNT-KS14, 1.08 mbsf g	6.23 ± 0.19	
			MNT-KS14, 1.23 mbsf a	9.97 ± 0.3	
			MNT-KS14, 1.23 mbsf b	9.07 ± 0.35	
			MNT-KS14, 1.48 mbsf	13.60 ± 1.1	
			MNT-KS14, 1.67 mbsf a	11.32 ± 0.51	
			MNT-KS14, 1.67 mbsf b	9.04 ± 0.39	
13	the Niger Delta	667	USN 12-1	21.6 ± 0.4	Ruffine et al., 2013
			USN 12-2	21.0 ± 0.6	
			USN 13-1	7.7 ± 0.4	
			USN 13-2	6.3 ± 0.2	
			USN 13-3	5.9 ± 0.2	
14	the northern South China Sea	328 - 400	HS4aDG-1-b	195 ± 22	Tong et al., 2013
			HS4aDG-1-d	258 ± 10	
		350 - 380	HS4DG-core	152 ± 5	
			HS4DG-rim	330 ± 24	
		498	TVG1-1-a	74 ± 15	
		484	TVG2-a	63 ± 15	
		473	TVG3-1-b	77 ± 17	

			TVG3-2-a	64 ± 12	
			TVG3-2-hole	66.0 ± 0.2	
			TVG3-2-lining	65.8 ± 0.3	
15	the South China Sea	473 - 498	TVG1-7 B	71.6 ± 10.8	Han et al., 2014
			TVG2-1B	64.4 ± 0.8	
			TVG3-3B	64.0 ± 2.9	
		530 - 560	TVG14-C1-1B	144.5 ± 12.7	
			TVG14-C1-1C	85 ± 77	
		765- 785	TVG9-C4B	55.1 ± 1.9	
			TVG11-C2-1	34.1 ± 0.7	
			TVG11-C2-5A	46.5 ± 0.5	
			TVG11-C2-5B	47.0 ± 0.5	
16	the Central American forearc	1225	129/0-16 (1.4cm)	56.5 ± 0.7	Liebetrau et al., 2014
			129/0-16 (1.7cm)	65.4 ± 0.7	
			129/0-16 (1.5cm)	65.6 ± 1.6	
			129/0-16 (3.4cm)	69.1 ± 0.8	
			129/0-16 (4.1cm)	67.4 ± 0.8	
			129/0-16 (3.3cm)	67.8 ± 0.9	
			129/0-16 (5cm)	63.2 ± 0.8	
			129/0-16 (12.6cm)	47.3 ± 0.6	
			129/0-38 (27.2cm)	47.9 ± 1.0	
			129/0-38 (27.5cm)	45.9 ± 1.4	
			129/0-38 (26.5cm)	32.1 ± 0.5	
			129/0-38 (27.8cm)	33.2 ± 0.5	
			129/0-38 (27.8cm)	26.4 ± 0.4	
			129/0-38 (27.8cm)	19.5 ± 0.3	
			129/0-38 (33.9cm)	36.6 ± 0.4	
			129/0-38 (35cm)	38.4 ± 0.5	
		783	157/0-15 (5cm)	75.3 ± 0.9	
			157/0-15 (6cm)	70.3 ± 1.3	
			157/23-49 (42.7cm)	65.5 ± 0.7	
			157/49-70 (61.8cm)	60.3 ± 0.6	
			157/49-70 (61cm)	55.8 ± 1.6	
			157/49-70 (67.8cm)	95.8 ± 1.4	
			157/49-70 (68.5cm)	95.1 ± 1.3	
		799	184/0-21 (6.5cm)	8.3 ± 0.2	
			184/21-30 (26.5cm)	19.9 ± 0.2	
			184/30-56 (51.6cm)	5.5 ± 0.1	
			184/30-56 (51cm)	5.6 ± 0.1	
			184/56-63 (59.9cm)	13.1 ± 0.2	
			184/56-63 (60.7cm)	11.2 ± 0.1	

		828	214/0-135 (9.5cm)	12.9 ± 0.2	
			214/0-135 (42.3cm)	13.0 ± 0.2	
			214/0-135 (42.5cm)	13.8 ± 0.2	
			214/135-167 (136.3cm)	0.25 ± 0.01	
			214/167-317 (199cm)	14.9 ± 0.2	
			214/167-317 (316cm)	15.5 ± 0.2	
17	the Niger delta margin	~ 1200	N2-KS-44_30 cm bulk	8.5 ± 0.2	Bayon et al., 2015
			N2-KS-44_75 cm bulk	9.3 ± 2.0	
			N2-KS-44_75 cm micromilled-1	12.4 ± 1.3	
			N2-KS-44_75 cm micromilled-2	4.8 ± 1.4	
			N2-KS-44_160 cm bulk	9.4 ± 2.4	
			N2-KS-44_180 cm micromilled-1	10.8 ± 2.7	
			N2-KS-44_260 cm bulk-1	15.6 ± 1.6	
18	the Makran convergent margin	1025	12315-3	0.01 ± 32	Himmler et al., 2015
		1475	12348-1	2.3 ± 3.9	
		1656	12338-2	15.5 ± 0.2	
			12338-13	16 ± 8	
		1823	12324-2	19.8 ± 5.0	
19	the Alvheim channel, central North Sea	126 - 148	13C-CARB-4 1	5.70 ± 0.02	Crémière et al., 2016a
			13C-CARB-4 2	5.78 ± 0.02	
			13C-CARB-4 3	5.75 ± 0.02	
			13C-CARB-4 4	6.09 ± 0.03	
			13C-CARB-4 5	5.90 ± 0.04	
			13C-CARB-8 1	3.46 ± 0.05	
			13C-CARB-8 2	5.09 ± 0.26	
			13C-CARB-8 3	4.44 ± 0.05	
			13C-CARB-11 1	4.77 ± 0.14	
			13C-CARB-11 2	4.12 ± 0.07	
			13C-CARB-11 3	5.31 ± 0.14	
			13C-CARB-11 4	5.59 ± 0.04	
			13C-CARB-11 5	4.45 ± 0.03	
			13C-CARB-16 1	1.55 ± 0.07	
			13C-CARB-16 2	1.19 ± 0.04	
			13C-CARB-16 3	0.98 ± 0.03	
			13C-CARB-16 4	1.94 ± 0.08	
			13C-CARB-16 5	1.28 ± 0.02	
			13C-CARB-17 1	1.15 ± 0.03	
			13C-CARB-17 2	1.02 ± 0.03	
			13C-CARB-17 3	1.86 ± 0.02	
			13C-CARB-17 4	1.23 ± 0.02	

			13C-CARB-17 5	0.81 ± 0.03	
			13C-CARB-17 6	1.21 ± 0.01	
			13C-CARB-17 7	1.35 ± 0.01	
20	the Norwegian margin	319	P1210001 1	13.66 ± 0.11	Crémière et al., 2016b
			P1210001 2	11.70 ± 0.05	
			P1210001 3	9.21 ± 0.54	
			P1210001 4	12.28 ± 0.28	
			P1210001 5	11.59 ± 0.11	
			P1210001 6	11.27 ± 0.04	
			P1210001 7	10.78 ± 0.52	
			P1210001 8	10.85 ± 0.15	
		320	P1210002 1	11.72 ± 0.11	
			P1210002 2	12.81 ± 0.11	
			P1210002 3	11.70 ± 0.16	
			P1210002 4	11.69 ± 0.26	
			P1210002 5	13.00 ± 0.13	
			P1210002 6	11.45 ± 0.52	
			P1210002 7	11.30 ± 0.61	
			P1210004 1	11.50 ± 0.45	
			P1210004 2	8.92 ± 0.05	
			P1210004 3	9.97 ± 0.04	
			P1210006 1	5.02 ± 0.03	
			P1210006 2	4.08 ± 0.02	
			P1210006 3	4.84 ± 0.04	
			P1210006 4	5.41 ± 0.07	
			P1210006 5	5.21 ± 0.04	
			P1210006 6	2.38 ± 0.03	
			P1210007 1	8.23 ± 0.05	
			P1210007 2	10.85 ± 0.06	
		403	P1210010 1	11.57 ± 0.09	
			P1210010 2	11.62 ± 0.14	
			P1210010 3	15.07 ± 1.42	
			P1210011 1	11.75 ± 0.06	
			P1210011 2	11.93 ± 0.06	
			P1210011 3	11.85 ± 0.22	
			P1210012 1	11.79 ± 0.09	
			P1210014 1	17.45 ± 0.74	
			P1210014 2	11.53 ± 0.33	
			P1210014 3	10.94 ± 0.06	
		391	P1210017 1	12.30 ± 0.23	
			P1210017 2	9.61 ± 0.04	

			P1210017 3	10.20 ± 0.04	
			P1210017 4	10.58 ± 0.05	
			P1210018 3	12.93 ± 1.04	
			P1210018 4	12.97 ± 2.52	
			P1210018 5	14.40 ± 0.55	
		393	P1210032 1	3.29 ± 0.42	
			P1210036 1	7.58 ± 0.39	
			P1210036 2	7.11 ± 0.09	
			P1210036 3	7.47 ± 0.10	
			P1210036 4	15.91 ± 4.17	
		218	Hola 1	9.91 ± 0.45	
			Hola 2	9.43 ± 0.85	
			Hola 3	6.06 ± 1.64	
			Hola 4	9.62 ± 0.27	
			Hola 5	9.60 ± 0.49	
			Hola 6	11.33 ± 0.63	
			Hola 7	9.54 ± 0.24	
			Hola 8	9.91 ± 0.16	
			Hola 9	10.91 ± 0.19	
			Hola 10	9.29 ± 0.17	
			Hola 11	9.34 ± 0.13	
21	off Pakistan, northern Arabian Sea	734	1	0.46 ± 4	Himmler et al., 2016
			2	0.13 ± 5	
			3	0.13 ± 12	
			4	0.14 ± 1	
			5	0.20 ± 2	
			7	0.42 ± 6	
22	Atlantic Margin	1455 - 1610	RB-13-682D	2.6 ± 1.4	Prouty et al., 2016
			RB-13-682E	3.3 ± 1.3	
			RB-13-682F	1.4 ± 0.3	
			RB-13-682G	1.2 ± 0.8	
			RB-13-682H	1.0 ± 0.7	
		~ 385	NF12-14D	14.8 ± 1.0	
			NF12-14E	15.4 ± 0.6	
			NF12-14F	14.7 ± 0.6	
			NF12-14G	15.4 ± 1.0	
			NF12-14H	15.7 ± 1.6	
23	the northern North Sea	~ 300	B53-2mørk	9.31 ± 1.92	Mazzini et al., 2017
			B53-2lys	10.65 ± 3.79	
24	northern Norway	~ 220	91-1 Hola 2-2-1	1.82 ± 0.06	Sauer et al., 2017
			91-2 Hola 2-2-2	1.72 ± 0.05	

			91-3 Hola 2-2-3	1.61 ± 0.02	
			91-4 Hola 2-2-4	2.08 ± 0.02	
			91-6 Hola 2-2-6	1.85 ± 0.03	
			96-1 2-2L 7	1.88 ± 0.33	
			96-2 2-2L 8	4.39 ± 1.63	
			96-4 2-2L 10	2.12 ± 0.05	
			91-7 Hola 5-2-1	4.17 ± 0.51	
			91-8 Hola 5-2-2	3.92 ± 0.03	
			91-9 Hola 5-2-3	4.32 ± 0.08	
			91-10 Hola 5-2-4	2.65 ± 0.02	
			91-11 Hola 5-2-5	3.78 ± 0.06	
			91-12 Hola 5-2-6	4.17 ± 0.13	
			91-13 Hola 5-2-7	2.66 ± 0.02	
			91-14 Hola 5-2-8	4.06 ± 0.04	
25	the Sea of Marmara	1107	DV04-CC01	0.58 ± 0.14	Çağatay et al., 2018
		1143	1661-R4	9.61 ± 2.40	
		1141	1661-R5	9.14 ± 2.29	
		1237	DV05-CC01	0.11 ± 0.03	
		326	1664-R2	0.53 ± 0.13	
26	the northern South China Sea	655	S03A_1	3.2 ± 0.4	Yang et al., 2018
			S03A_2	2.8 ± 1.1	
			S03A_3	3.1 ± 0.7	
			S03A_4	3.2 ± 0.5	
		638	S04F_1	5.5 ± 0.7	
			S04F_2	4.2 ± 2.5	
			S04F_3	4.2 ± 2.4	
27	the Arctic	1206	P1606001_B-B1	20.22 ± 0.43	Himmler et al., 2019
			P1606001_B-B1	17.65 ± 0.26	
		1203	P1606005-B-B2	17.22 ± 0.29	
			P1606005-B-B2	19.03 ± 0.87	
		1210	P1606010-1-C1	5.98 ± 0.53	
			P1606010-1-C2	12.84 ± 1.02	
		1207	P1606011-2-B2	6.07 ± 0.59	
			P1606012-1-B2	6.21 ± 0.28	
			P1606012-1-B2	7.73 ± 0.53	
			P1606012-1-B2	11.48 ± 0.86	
			P1606012-1-B2	4.72 ± 0.21	
			P1606012-1-B2	9.92 ± 0.71	
		1204	P1606023-B1-B2	16.39 ± 0.55	
			P1606023-B1-B2	12.14 ± 1.77	
			P1606023-B1-B2	20.22 ± 1.29	

			P1606023-B1-B2	14.70 ± 2.59	
		1210	GeoB21616-1-B-a	40.24 ± 0.28	
			GeoB21616-1-B-b	43.70 ± 0.79	
			GeoB21616-1-E-a	41.50 ± 0.27	
			GeoB21616-1-E-c	50.05 ± 1.43	
			GeoB21616-1-a	41.65 ± 0.61	
			GeoB21616-1-b	41.83 ± 0.58	
			GeoB21616-1-c	41.18 ± 0.75	
		1209	GeoB21637-1-B-b	143.95 ± 3.43	
			GeoB21637-1-A-b	172.77 ± 3.79	
			GeoB21637-1-B-a	142.62 ± 2.65	
			GeoB21637-1-A-b	141.15 ± 2.54	
			GeoB21637-1-B-a	142.05 ± 1.40	
			GeoB21637-1-B-b	150.24 ± 1.94	
			GeoB21637-1-C-a	156.25 ± 1.75	
			GeoB21637-1-C-a	132.54 ± 2.39	
			GeoB21637-1-E-a	160.74 ± 8.87	
			GeoB21637-1-E-b	142.99 ± 2.11	
			GeoB21637-1-O-a	143.07 ± 2.75	
			GeoB21637-1-O-b	142.47 ± 1.88	
			GeoB21637-1-Q-a	158.19 ± 2.60	
			GeoB21637-1-V-a	136.56 ± 2.09	
			GeoB21637-1-W-b	152.65 ± 2.79	

References:

Aharon, P., Schwarcz, H.P., & Roberts, H.H. (1997). Radiometric dating of submarine hydrocarbon seeps in the Gulf of Mexico. *Geological Society of America Bulletin, 109*, 568–579.

Bayon, G., Loncke, L., Dupré, S., Caprais, J.-C., Ducassou, E., Duperron, S., Etoubleau, J., Foucher, J.-P., Fouquet, Y., Gontharet, S., Henderson, G.M., Huguen, C., Klaucke, I., Mascle, J., Migeon, S., Roy, O.-L.K., Ondréas, H., Pierre, C., Sibuet, M., Stadnitskaia, A., & Woodside, J. (2009a). Multi-disciplinary investigation of fluid seepage on an unstable margin: The case of the Central Nile deep sea fan. *Marine Geology, 261*, 92–104.

Bayon, G., Henderson, G.M., & Bohn, M. (2009b). U-Th stratigraphy of a cold seep carbonate crust. *Chemical Geology, 260*, 47–56.

Bayon, G., Stéphanie, D., Ponzevera, E., Etoubleau, J., Chéron, S., Pierre, C., Mascle, J., Boetius, A., & de Lange, G.J. (2013). Formation of carbonate chimneys in the Mediterranean Sea linked to deep-water oxygen depletion. *Nature Geoscience, 6*, 755–760.

Bayon, G., Henderson, G.M., Etoubleau, J., Caprais, J.-C., Ruffine, L., Marsset, T., Dennielou, B., Cauquil, E., Voisset, M., & Sultan, N. (2015). U-Th isotope constraints on gas hydrate and pockmark dynamics at the Niger delta margin. *Marine Geology, 370*, 87–98.

Çağatay, M.N., Yıldız, G., Bayon, G., Ruffine, L., & Henry, P. (2018). Seafloor authigenic carbonate crusts along the submerged part of the North Anatolian Fault in the Sea of Marmara: Mineralogy, geochemistry, textures and genesis. *Deep Sea Research Part II: Topical Studies in Oceanography*, *153*, 92–109.

Cheng, H., Edwards, R.L., Shen, C., Polyak, V.L., Asmerom, Y., Woodhead, J., Hellstrom, J., Wang, Y., Kong, X., Spötl, C., Wang, X., & Alexander Jr, E.C. (2013). Improvements in ^{230}Th dating, ^{230}Th and ^{234}U half-life values, and U–Th isotopic measurements by multi-collector inductively coupled plasma mass spectrometry. *Earth and Planetary Science Letters*, *371-372*, 82–91.

Crémière, A., Bayon, G., Ponzevera, E., & Pierre, C. (2013). Paleo-environmental controls on cold seep carbonate authigenesis in the Sea of Marmara. *Earth and Planetary Science Letters*, *376*, 200–211.

Crémière, A., Lepland, A., Chand, S., Sahy, D., Kirsimäe, K., Bau, M., Whitehouse, M.J., Noble, S.R., Martma, T., Thorsnes, T., & Brunstad, H. (2016a). Fluid source and methane-related diagenetic processes recorded in cold seep carbonates from the Alvheim channel, central North Sea. *Chemical Geology*, *432*, 16–33.

Crémière, A., Lepland, A., Chand, S., Sahy, D., Condon, D.J., Noble, S.R., Martma, T., Thorsnes, T., Sauer, S., & Brunstad, H. (2016b). Timescales of methane seepage on the Norwegian margin following collapse of the Scandinavian Ice Sheet. *Nature Communications*, *7*, 11509.

Feng, D., Roberts, H.H., Cheng, H., Peckmann, J., Bohrmann, G., Edwards, R.L., & Chen, D. (2010). U/Th dating of cold-seep carbonates: An initial comparison. *Deep-Sea Research Part II: Topical Studies in Oceanography*, *57*, 2055–2060.

Han, X., Suess, E., Liebetrau, V., Eisenhauer, A., & Huang, Y. (2014). Past methane release events and environmental conditions at the upper continental slope of the South China Sea: constraints by seep carbonates. *International Journal of Earth Sciences*, *103*, 1873–1887.

Himmler, T., Birgel, G., Bayon, G., Pape, T., Ge, L., Bohrmann, G., & Peckmann, J. (2015). Formation of seep carbonates along the makran convergent margin, northern Arabian sea and a molecular and isotopic approach to constrain the carbon isotopic composition of parent methane. *Chemical Geology*, *415*, 102–117.

Himmler, T., Bayon, G., Wangner, D., Enzmann, F., Peckmann, J., & Bohrmann, G. (2016). Seep-carbonate lamination controlled by cyclic particle flux. *Scientific Reports*, *6*, 37439.

Himmler, T., Sahy, D., Martma, T., Bohrmann, G., Plaza-Faverola, A., Bünz, S., Condon, D.J., Knies, J., & Lepland, A. (2019). A 160,000-year-old history of tectonically controlled methane seepage in the Arctic. *Science Advances*, 5: eaaw1450.

Jaffey, A.H., Flynn, K.F., Glendenin, L.E., Bentley, W.C., & Essling, A.M. (1971). Precision measurement of half-lives and specific activities of ^{235}U and ^{238}U. *Physical review C 4*, 1889–1906.

Kutterolf, S., Liebetrau, V., Mörz, T., Freundt, A., Hammerich, T., & Garbe-Schönberg, D. (2008). Lifetime and cyclicity of fluid venting at forearc mound structures determined by tephrostratigraphy and radiometric dating of authigenic carbonates. *Geology*, *36*, 707–710.

Lalou, C., Fontugne, M., Lallemand, S.E., & Lauriat-Rage, A. (1992). *Calyptogena*-cemented rocks and concretions from the eastern part of Nankai accretionary prism:

Age and geochemistry of uranium. *Earth and Planetary Science Letters, 109*, 419–429.
Liebetrau, V., Eisenhauer, A., & Linke, P. (2010). Cold seep carbonates and associated cold-water corals at the Hikurangi Margin, New Zealand: New insights into fluid pathways, growth structures and geochronology. *Marine Geology, 272*, 307–318.
Liebetrau, V., Augustin, N., Kutterolf, S., Schmidt, M., Eisenhauer, A., Garbe-Schönberg, D., & Weinrebe, W. (2014). Cold-seep-driven carbonate deposits at the Central American forearc: contrasting evolution and timing in escarpment and mound settings. *International Journal of Earth Sciences, 103*, 1845–1872.
Mazumdar, A., Dewangan, P., Joäo, H.M., Peketi, A., Khosla, V.R., Kocherla, M., Badesab, F.K., Joshi, R.K., Roxanne, P., Ramamurty, P.B., & Karisiddaiah, S.M. (2009). Evidence of paleo–cold seep activity from the Bay of Bengal, offshore India. *Geochemistry, Geophysics, Geosystems, 10*, Q06005, doi:10.1029/2008GC002337.
Mazzini, A., Svensen, H.H., Forsberg, C.F., Linge, H., Lauritzen, S.-E., Haflidason, H., Hammer, Ø., Planke, S., & Tjelta, T.I. (2017). A climatic trigger for the giant Troll pockmark field in the northern North Sea. *Earth and Planetary Science Letters, 464*, 24–34.
Prouty, N.G., Sahy, D., Ruppel, C.D., Roark, E.B., Condon, D., Brooke, S., Ross, S.W., & Demopoulos, A.W.J. (2016). Insights into methane dynamics from analysis of authigenic carbonates and chemosynthetic mussels at newly-discovered Atlantic Margin seeps. *Earth and Planetary Science Letters, 449*, 332–344.
Ruffine, L., Caprais, J.-C., Bayon, G., Riboulot, V., Donval, J.-P., Etoubleau, J., Birot, D., Pignet, P., Rongemaille, E., Chazallon, B., Grimaud, S., Adamy, J., Charlou, J.-L., & Voisset, M. (2013). Investigation on the geochemical dynamics of a hydrate-bearing pockmark in the Niger Delta. *Marine and Petroleum Geology, 43*, 297–309.
Sauer, S., Crémière, A., Knies, J., Lepland, A., Sahy, D., Martma, T., Noble, S.R., Schönenberger, J., Klug, M., & Schubert, C.J. (2017). U-Th chronology and formation controls of methane-derived authigenic carbonates from the Hola trough seep area, northern Norway. *Chemical Geology, 470*, 164–179.
Teichert, B.M.A., Eisenhauer, A., Bohrmann, G., Haase-Schramm, A., Bock, B., & Linke, P. (2003). U/Th systematics and ages of authigenic carbonates from Hydrate Ridge, Cascadia Margin: Recorders of fluid flow variations. *Geochimica Et Cosmochimica Acta, 67*, 3845–3857.
Tong, H., Feng, D., Cheng, H., Yang, S., Wang, H., Min, A.G., Edwards, R.L., Chen, Z., & Chen, D. (2013). Authigenic carbonates from seeps on the northern continental slope of the South China Sea: New insights into fluid sources and geochronology. *Marine and Petroleum Geology, 43*, 260–271.
Watanabe, Y., Nakai, S., Hiruta, A., Matsumoto, R., & Yoshida, K. (2008). U–Th dating of carbonate nodules from methane seeps off Joetsu, Eastern Margin of Japan Sea. *Earth and Planetary Science Letters, 272*, 89–96.
Yang, K., Chu, F., Zhu, Z., Dong, Y., Yu, X., Zhang, W., & Ma, W. (2018). Formation of methane-derived carbonates during the last glacial period on the northern slope of the South China Sea. *Journal of Asian Earth Sciences, 168*, 173–185.